Surface & Coatings Technology 464 (2023) 129540

Contents lists available at ScienceDirect

Surface & Coatings Technology

journal homepage: www.elsevier.com/locate/surfcoat

Full length article

Deposition and characterisation of *c*-axis oriented AlScN thin films via microwave plasma-assisted reactive HiPIMS

L. Lapeyre [a,b,*], C. Hain [a,b], P. Sturm [c], J. Metzger [c], A. Borzì [d], K. Wieczerzak [b], P. Raynaud [e], J. Michler [b], T. Nelis [a,b]

[a] Bern University of Applied Sciences, Institute for Applied Laser, Photonics and Surface Technologies ALPS, Quellgasse 21, 2502 Biel/Bienne, Switzerland
[b] Empa, Swiss Federal Laboratories for Materials Science and Technology, Laboratory for Mechanics of Materials and Nanostructures, Feuerwerkerstrasse 39, 3602 Thun, Switzerland
[c] TOFWERK, Schorenstrasse 39, 3645 Thun, Switzerland
[d] Center for X-ray Analytics, Swiss Federal Laboratories for Materials Science and Technology, Empa, Überlandstrasse 129, 8600 Dübendorf, Switzerland
[e] Laboratoire Plasma et Conversion d'Energie (LAPLACE), Université de Toulouse, CNRS, INPT, UPS, 31062 Toulouse, France

ARTICLE INFO

Keywords:
Aluminium scandium nitride
HiPIMS
Microwave plasma
Plasma diagnostics
Thin films
Material characterisation

ABSTRACT

In this work, we demonstrate that highly oriented c-axis aluminium scandium nitride (AlScN) piezoelectric thin films can be deposited via microwave plasma-assisted reactive high power impulse magnetron sputtering (MAR-HiPIMS), without the necessity of substrate heating. A combination of in situ plasma diagnostics, i.e. time-of-flight mass spectrometry (ToF-MS), modified quartz crystal microbalance (m-QCM), and magnetic field measurements allowed to optimise the deposition conditions, in turn maximising the nitrogen supply and ionic flux at the substrate region, while maintaining stable discharge conditions. The AlScN thin films synthesised in this study were deposited as chemically gradient coatings with varying levels of scandium doping, and were characterised using scanning electron microscopy (SEM), energy-dispersive X-ray spectroscopy (EDX), and X-ray diffraction (XRD). Obtaining highly textured films was made possible with the addition of microwave plasma to the optimised HiPIMS discharge, where the wurtzite AlScN films (with up to 20 at. % Sc) exhibited a stronger texture in the (0002) orientation compared to films prepared without microwave plasma. Additionally, the use of a microwave plasma led to a significant decrease in oxygen content in the films and increase in nitrogen content, ensuring stoichiometric compositions. Based on the results mentioned above, it is expected that the AlScN thin films fabricated via MAR-HiPIMS would exhibit a strong piezoelectric response.

1. Introduction

Aluminium nitride (AlN) films have been widely studied for their piezoelectric properties, which have made them attractive for various applications, e.g. radiofrequency filters or surface acoustic wave sensors [1–3]. The main prerequisites for good quality piezoelectric thin films are highly textured and dense structures, for efficient electromechanical conversion. This is an important aspect as high energy harvesting efficiency is required for most applications in microelectromechanical systems (MEMS) [2]. In an attempt to improve the piezoelectric properties of AlN, it was found that introducing scandium into the wurtzite structure of AlN increases its d_{33} piezoelectric response 5-fold, as observed for $Al_{57}Sc_{43}N$ produced via reactive radio frequency (RF) co-sputtering [3]. In another study [4], the transverse response d_{31} was reported to increase by a factor 2.5 for $Al_{58}Sc_{42}N$ compared to AlN. This significant improvement in electromechanical conversion efficiency, highly attractive for the development of MEMS, explains the piezoelectric community's increasing interest in AlScN and in the means of obtaining high quality thin films.

Thin films of AlN have been deposited by a range of techniques, including metalorganic chemical vapour deposition (MOCVD) [5] and physical vapour deposition (PVD) techniques, e.g. direct current magnetron sputtering (DCMS) [6,7] and high power impulse magnetron sputtering (HiPIMS) [8–11]. With a wider range of tuneable process parameters, the possibility of depositing at lower temperatures and obtaining films with lower surface roughness than via CVD, magnetron sputtering has become the method of choice for the deposition of AlN and AlScN films. Additionally, magnetron sputtering has been reported

* Corresponding author at: Feuerwerkerstrasse 39, 3603 Thun, Switzerland.
E-mail address: leo.lapeyre@empa.ch (L. Lapeyre).

https://doi.org/10.1016/j.surfcoat.2023.129540
Received 5 December 2022; Received in revised form 12 April 2023; Accepted 15 April 2023
Available online 1 May 2023

to provide the highest AlScN piezoelectric coefficient on flat substrates [3,11,12]. The high density of the deposited films, beneficial for piezoelectric materials, is another advantage of sputtering, especially in the case of HiPIMS [13]. Moreira et al. [10] showed that substrate heating did not improve the properties of AlN films synthesised via HiPIMS, as the samples produced at room temperature presented similar crystallinity compared to samples prepared at 400 °C. This result was attributed to an increased ad-atom mobility at the substrate surface due to the significant amount of ions generated by means of the HiPIMS discharge, which has been described in more detail by Anders et al. based on the structure zone diagram [14].

Despite the increasing number of publications on AlScN, the majority of reported studies focus solely on the properties of the deposited films, without considering the effects of the deposition conditions. This leaves a considerable gap in the understanding behind the mechanisms of AlScN film growth and, in turn, limits their optimisation and tailoring possibilities. Furthermore, to the best of the authors' knowledge, AlScN deposition via HiPIMS has not yet been reported. HiPIMS is an attractive deposition method for piezoelectric and ferroelectric thin films (as shown recently for AlScN [15–17]) as it provides the possibility for reaching high densities, reducing the likelihood of charge carriers being trapped and creating leakage current. Increased film density can also reduce the pathways for charge carriers to move through a material, further reducing the leakage current. Additionally, Yassine et al. [16] have reported that smoother coatings exhibit increased polarity, which suggests that the smooth morphology of HiPIMS-deposited thin films may be advantageous for dielectric applications. Overall, the low surface roughness, high density, and controlled film growth of HiPIMS-deposited thin films make this technique an interesting option for the development of dielectric thin films with enhanced properties, such as high piezoelectric response and low dielectric loss.

In this work, AlScN films (with Sc various concentrations) were fabricated via reactive HiPIMS (R-HiPIMS) in the presence of an electron cyclotron resonance (ECR) microwave (MW) plasma. Combining magnetron sputtering and MW-ECR sources was first introduced in the context of ionised PVD (IPVD) [18–20] in the 1990s (see recent review paper of Gudmudsson et al. [21]). Later on, Stranak et al. demonstrated that combining HiPIMS discharges with RF-driven (f_{RF} = 13.56 MHz) ECR plasma sources [22,23] is advantages for low-pressure applications and for modifying sputtered ionic fluxes. In our work, we employ MWs (f_{MW} = 2.45 GHz) to ensure high availability of reactive (activated) nitrogen close to the growing film, e.g. through excitation/ionisation/dissociation of the molecular species or further ionisation of the atomic species. In turn, this can lead to improved material stoichiometry and reduced contamination incorporation. The use of microwave plasma-assisted reactive HiPIMS (MAR-HiPIMS) was successfully performed by Hain et al. for the fabrication of preferentially-textured indium nitride (InN) thin films [24].

In the scope of this work, two main process parameters were considered. Firstly, the influence of the magnetrons' magnetic field configuration on the discharge current and ionic flux density near the substrate was investigated, with the aim of maximising ionic species generation at both the target and substrate regions. Secondly, the nitrogen flow was optimised to run the discharge in the so-called transition regime [25], allowing to deposit stoichiometric films while ensuring a relatively high deposition rate. To characterise the influence of process parameters on the deposition environment, modified quartz crystal microbalance (m-QCM) and a time-of-flight mass spectrometer (ToF-MS) were used for in situ diagnostics. The process parameters were carefully selected to maximise deposition rates and discharge peak currents, to facilitate the generation of a high amount of energetic particles. Next, compositionally graded AlScN films were deposited and characterised by means of scanning electron microscopy (SEM), energy dispersive X-ray spectroscopy (EDX), and X-ray diffraction (XRD) to determine the influence of the volume MW plasma filling the entire volume of the deposition chamber, on the films' microstructure and properties, as a function of the film's chemical composition, substrate heating, substrate biasing and Sc content.

2. Materials and methods

2.1. Deposition setup and film fabrication

AlScN thin films were deposited via R-HiPIMS in a face-to-face magnetron co-sputtering configuration using 2 planar magnetrons assemblies (Korvus Technology, UK), with a tilt of 27° in respect to the z-axis of the HexL hexagonal vacuum chamber (Korvus Technology, UK). The pumping system was composed of a primary dry scroll pump NXDS10i (Edwards, UK), and a turbomolecular pump HiPACE 700 (Pfeiffer Vacuum, Germany) enabling to reach a base pressure of 10^{-4} Pa. The argon and nitrogen gas supplies were controlled via a 200 and a 50 sccm mass-flow controller (Teledyne Hastings Instruments, USA), respectively. Two sets of SmCo magnets in unbalanced configuration (type II) were installed in the magnetrons assemblies to vary the generated magnetic field. Both sets had a central and annular magnet, with diameters of ∅ 10.1 and 51 mm, respectively. However, the annular magnets were characterised by different thicknesses, i.e. 6 mm and 7.5 mm. For magnetic field analysis (see 3.1.1), a portable magnetic field mapping system (M3D-2A-PORT, Senis, Switzerland) was used over an area of 68 × 56 mm^2 over the magnets. The magnetrons were powered by 1 kW HiPSTER 1 pulsing units (Ionautics, Sweden), driven by programmable DC power supplies (SL-series Magna-Power, USA). Two self-matching electron cyclotron resonance (ECR) "Aura-Wave" coaxial microwave sources (Sairem, France) [26,27] were installed 140 mm from the centre of the substrate holder, as depicted in Fig. 1A. Each source was powered by a solid-state microwave generator at 2.45 GHz, with a 100 MHz frequency tuning window for impedance matching. The highest plasma density forms at the Aura-wave source in a donut-shape manner.

The substrates, onto which AlScN films were deposited, were 4-in. p-type (100)-orientated silicon wafers (MicroChemicals, Germany). The target-to-substrate distance was set to 13 cm. Prior to deposition, the wafers were subjected to a pre-treatment process, which consisted of exposing them to a microwave Ar plasma for 10 min at 0.2 Pa to remove the native silicon oxide layer and surface contaminations. The MW sources (situated approx. 12 cm from the magnetrons) were operated at 50 W each, with the substrate rotated at 15 rpm and biased at −150 V to accelerate the Ar ions bombarding the wafer. In situ ellipsometry measurements confirmed the total etching of the native SiO_2 layer, with a 4 nm amorphous Si layer being generated (results not included in this study).

The discharges of the ∅ 50 × 3 mm Al (99.999 wt%) and Sc (99.9 wt %) targets (Ampere Industry, France) were controlled by regulating the average power (Al at 200 W, Sc at 160 W) and were sputtered at a frequency of 250 Hz. Furthermore, the HiPIMS discharges (Al: 50 μs, Sc: 60 μs) and substrate bias were synchronised using an external synchronisation unit (Ionautics, Sweden). The triggering sequence is shown in Fig. 1C. Prior to film deposition, the targets were pre-sputtered for 2 min under magnetron shutters to remove any oxides or surface contaminants. The gas flows were adjusted to 60 and 20 sccm for Ar and N_2, respectively, and the pressure was kept at 0.6 Pa using an in-house developed butterfly valve. During deposition, the power on each MW plasma source was set to 100 W. For investigating the influence of Sc content on the films' microstructure, chemically-graded AlScN films were deposited. To this end, the sample holder was rotated in a symmetrical manner, turning it back and forth through a total angle of 90°, i.e. ±45° around the initial position, at a speed of 10 rpm. Two deposition temperatures (controlled using a ∅ 1 × 50 mm custom-made microwave plasma-resistant temperature probe from Mesurex, France) were applied, i.e. without substrate heating (approx. 150 °C) and with heating at 400 °C. Each process lasted 2.5 h to reach a film thickness of approx. 500 nm.

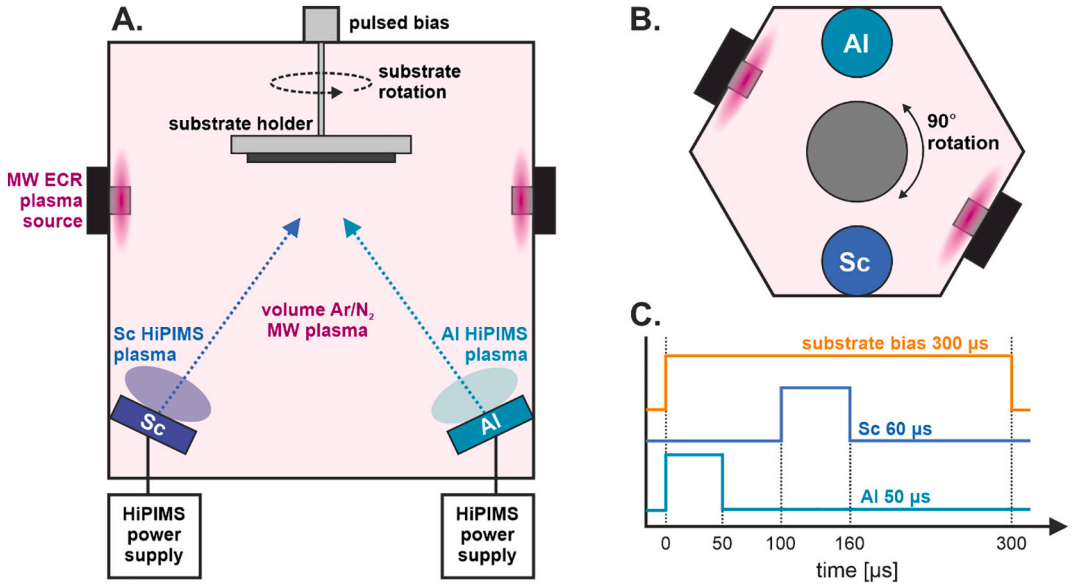

Fig. 1. Schematic of the used system configuration: A. side view, B. top view. MW sources are situated at 140 mm from substrate centre. The substrate holder is symmetrically rotated back and forth in a 90° rotation to generate in-plane AlScN chemical gradient. Ar/N_2 mixture is introduced through gas lines situated inside magnetrons, below the targets level. C. triggering sequence for the substrate bias and Al and Sc magnetrons.

2.2. In situ plasma diagnostics

Ionised flux fraction measurements were performed using a ∅ 100 mm Quantum™ System m-QCM probe (Impedans, Ireland), where a quartz crystal microbalance (QCM) is combined with a retarding field energy analyser (RFAE), comprising of 4 grids and measures ion energies and ionic flux densities, see [28] for details.

Mass spectra were acquired using a prototype time-of-flight mass analyser instrument (TOFWERK, Switzerland) which combines a commercial mass analyser (CTOF module) with an electrostatic ion energy analyser [24].The mass analyser used a flight length of approximately 370 mm, providing simultaneous mass-to-charge ratios between 1 and 500 Th. For the experimental conditions, a mass resolving power of 500 for low mass to charge ratios (e.g. Ar^{2+}) and 1000 for heavier ions (e.g. Hf^{+} 180 Th) was observed. The instrument's ion sampling aperture, a 30 µm orifice (ground potential), was positioned at the height of the substrate to analyse the incident ions during sputtering. The residual pressure within the sampling ion optics was kept below 5×10^{-3} Pa to ensure that charge transfer and recombination reactions can be neglected.

The voltage and current output signals supplied by the HiPSTERs were monitored using a mixed signal oscilloscope (Tektronix, USA). Data were acquired using the averaging mode, based on 128 pulses.

2.3. Film characterisation

Surface morphology and fracture cross-sections were imaged using a Hitachi S-4800 high-resolution cold field emission (CFE) SEM (Hitachi High-Tech Corporation, Japan). Energy dispersive X-ray measurements were performed using a Zeiss Sigma VP SEM, employing an X-Max 80 detector (Oxford Instrument, UK).

Structural analysis was performed via XRD using a Bruker D8 Discover diffractometer (Bruker, USA) with CuKα1 and CuKα2 radiations (λ = 1.5406 and 1.54439 Å, respectively). The θ-2θ scans were performed in the range from 20 to 90°, with an offset of 2° from the symmetrical diffraction geometry (Bragg-Brentano configuration) to avoid the (400) reflection of the (100)-oriented single crystal Si substrate. The grazing incidence measurements were performed using the same device, in the range from 20° to 80° with a beam incident angle of 1°. The measurement conditions were: 40 kV voltage, 40 mA current, step size of 0.02° and the collection time at each step was 2 s. For texture analysis, pole figures were performed using a Malvern Panalytical Empyrean instrument (Netherlands), exploiting Cu-Kα radiation (λ = 1.5418 Å) and optics to condition the incident beam.

3. Results and discussion

3.1. Plasma diagnostics

3.1.1. Influence of magnetic field strength

For both magnet configurations, identical centre magnets were used, however, the thickness of the annular magnets differed, i.e. 6 and 7.5 mm. Therefore, prior to chamber installation, the magnetic field lines of both configurations were mapped in the *xz* planes above the target's surface. An example map for the 7.5 mm annular magnet is shown in Fig. 2.

For both magnet sets, the null point is situated at 23 mm from the

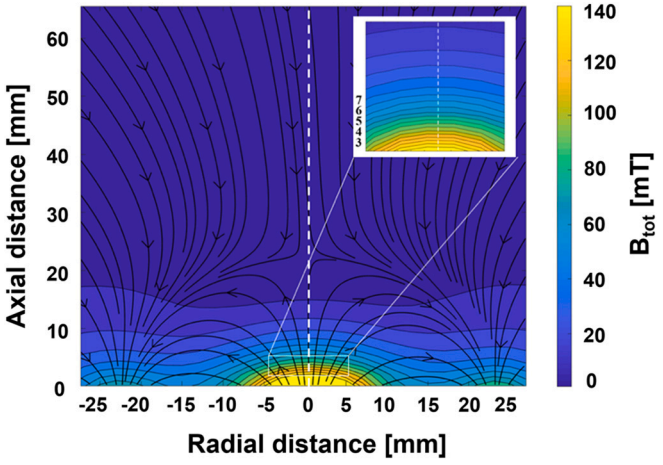

Fig. 2. Magnetic field map for the 7.5 mm annular magnet configuration, including streamlines for visualising the magnetic flux' direction and contour plots of the magnetic field norm B_{tot}. The inset image highlights the strength gradient near the target. The mapping was initiated at the height the racetrack, i.e. 4 mm above the central magnet.

central magnet's surface on the symmetry axis of the magnetron system, indicating a strongly unbalanced configuration. At 4 mm above the central magnets (at the target), the 6 mm and 7.5 mm annular magnet configurations had a magnitude of 80 mT (weaker field) and 100 mT (stronger field), respectively. The field gradient close to the target surface, between 3 and 5 mm, is considered as strong, as the magnetic field strength drops by 40 % across this distance. Therefore, the magnetic field present at the target's surface will strongly depend on its thickness, which continuously changes with sputtering. Consequently, the number of electrons trapped in the racetrack region will experience significant variations, which implies that the sputtering discharge conditions will also vary, e.g. higher peak currents for thinner targets, or higher deposition rates at a given power. Next, the influence of the two magnetic configurations on the sputtering characteristics were studied by following the differences in HiPIMS I(*V,t*) curves and ionic flux densities reaching the substrate. As can be seen in Fig. 3, the magnetic field strength has a significant impact on the discharge behaviour. The stronger magnetic field allowed for a 39 % increase in the peak current at constant voltage and pressure, in comparison to the weaker one. The ion flux density, as measured by the m-QCM, was significantly higher for all tested nitrogen flows, with the discharge operated in constant power mode. Additionally, the R-HiPIMS discharge could be stabilised at N_2 flows exceeding 20 sccm.

Both the ion flux density and the deposition rate (from 0.043 to 0.051 nm/s) increased when using the stronger field configuration. In this work, the increased ion flux did not cause significantly higher back attraction, which could reduce overall deposition rates, as reported in earlier works [29,30]. This difference may be caused by the small null point distance of 23 mm compared to $\leq$50 mm for the magnetrons used in previous works. In the context of AlScN films, high currents and high ionic flux densities are desired to maximise the activation (excitation/ionisation/dissociation) of nitrogen. The higher deposition rates observed using the stronger field configuration is also beneficial for the thin film properties, as it will reduce the incorporation of oxygen during deposition. Therefore, the stronger field magnet setup (mounted in open field configuration [7]) was used for both target materials during subsequent film fabrication.

3.1.2. *Effect of nitrogen flow*

The shape of the I(*V,t*) pulse discharge curves, as well as the deposition rates and ionised fractions were recorded at various reactive gas flows to characterise the different discharge stages encountered during reactive sputtering [25]. Fig. 4 shows HiPIMS I(*V,t*) curves and deposition rates obtained when sputtering from the Al target, with the N_2 flow varying from 0 to 24 sccm (60 sccm Ar flow, 0.6 Pa pressure). The HiPIMS voltage was limited to 750 V, the average power to 200 W and the pulse repetition frequency was set to 250 Hz, with a pulse width of 50 μs. No significant hysteresis effect was observed when varying the N_2 flow.

Upon surface nitriding, the Al target's secondary electron emission yield (γ_{see}) significantly increases [31], which contributes to the observed peak current increase (at constant voltage) from 16 A to 40 A already at low N_2 flows (8 and 12 sccm) i.e. < 16 % of the total gas flux. The general shape of the current curve does not greatly change. The deposition rate remains constant, despite the increase in power and measured ionised fraction. Therefore, it would seem that for this N_2 flow range, the sputtering of the Al target is in the *metallic regime* [25]. Further increasing the N_2 flow rate up to 20 sccm (25 % total gas flux) did not influence the peak current or the shape of the discharge current curve. A small increase in deposition rate was detected, possibly caused by the increased incorporation of N in the deposited film, as well as an increase in the ionised flux, despite a constant discharge current. The behaviour of the sputtered Al target in this N_2 flow range (12–20 sccm) is assigned to the *transition regime*. For N_2 flow rates >20 sccm, the discharge conditions changed considerably. When operating the discharge in constant power mode, the peak current increased, while the discharge voltage decreased. The current increase observed during the first 15 μs of the 50 μs pulse is slow compared to the increase observed for lower N_2 flows. This effect, already reported in literature [32], is the result of metallic Al species remaining from the previous pulse. This allows the current onset to increase more quickly compared to higher reactive gas flows, where the amount of remaining species from the previous pulse is decreased (Fig. 4A). This is a direct consequence of compound layer formation on the sputter target's surface with increased N_2 flows. This regime is commonly referred to as the *poisoned* or *compound regime*. Here, a high ionised fraction of sputtered species is observed. Fekete et al. [32], who investigated the influence of reactive gas flow on the ionised fraction of Ti via OES, observed a stronger decrease in neutral Ti compared to its ionised form, resulting in a higher ionised fraction in the poisoned mode (75 % in the *metallic regime* vs 89

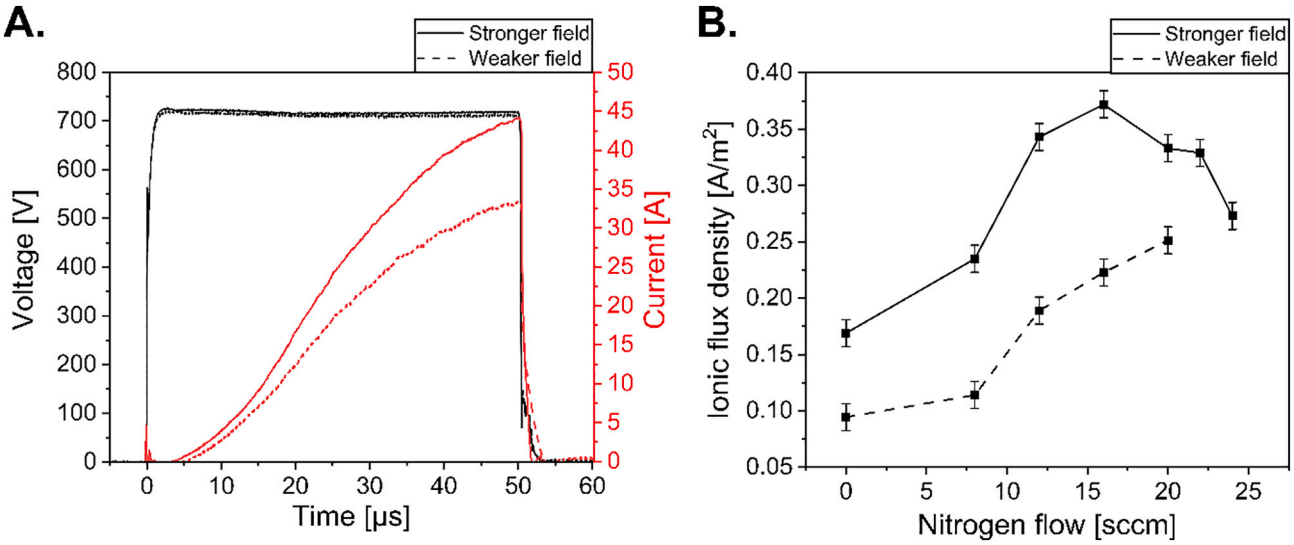

Fig. 3. A. Pulse shapes recorded for the stronger (7.5 mm) and weaker (6 mm) field magnet configurations for a N_2 flow of 20 sccm, at an average power of 200 W and at 250 Hz frequency, without MW plasma; B. ionic flux densities measured at the substrate region for different N_2 flows. From 0 to 8 sccm, the discharge was voltage-regulated at 750 V. For flows above 8 sccm, the discharge was power- regulated (200 W), enabling the discharge voltage and current to evolve when increasing nitrogen flow and clearly distinguish the different reactive sputtering discharge regimes. Another purpose for selecting the power-mode was to limit magnetron's overheating issues when exceeding 200 W, generating plasma arcing and instabilities.

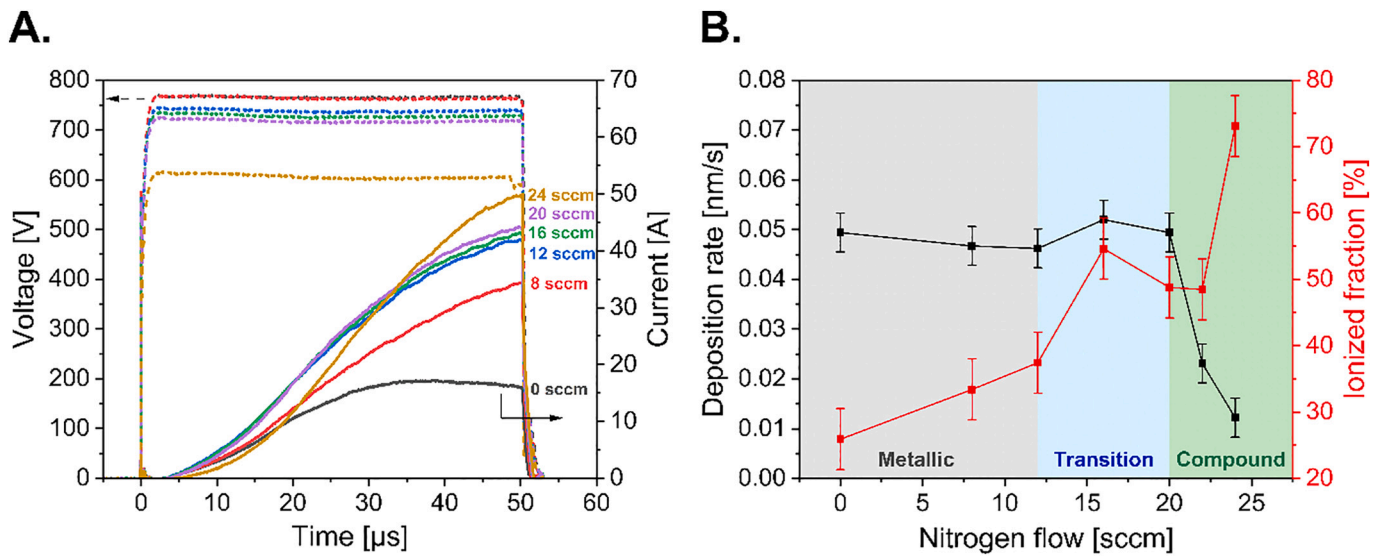

Fig. 4. A. HiPIMS I(V,t) curves for the Al discharge; B. deposition rates and ionised fractions measured during Al R-HiPIMS, while varying the N_2 flow from 0 to 24 sccm, with a constant Ar flow of 60 sccm; Similarly to discharge conditions depicted in Fig. 4 caption, sputtering was first voltage-limited at −750 V for the N_2 flow range of 0 to 8 sccm, whereas for higher N_2 flows it was power-limited at 200 W.

% in the *poisoned regime*). They attributed this increase in ionised fraction to a higher recycling of gas ions in the discharge. As the flux of atoms leaving the target is lower at high N_2 flows (as seen from the decreased deposition rate), the gas ions are able to remain in the target region for a longer time (i.e. longer residual time), increasing the probability for collisional ionisation of the sputtered species. This leads to an increase in peak current and ionised fraction in the compound mode.

Based on the obtained results, the nitrogen flow rate selected for further studies and film depositions was 20 sccm. Situated at the upper limit of the *transition regime*, stoichiometric films are expected to be produced and the discharge shows one of the highest deposition rates for all studied flows. The power-limited mode (200 W) was selected to avoid target overheating and plasma instabilities during the deposition process of samples characterised in Section 3.2.

3.1.3. *Microwave plasma influence on HiPIMS discharge*

The influence of the MW plasma can be seen on the behaviour of the Al target's discharge current (Fig. 5). The discharge was regulated by a constant voltage of −750 V, allowing the average power to vary. With the MW plasma on, the current shape shows a faster current increase after 10 µs and the peak current experiences an increase of approx. 4 A.

The volume MW plasma is a continuous source of charged species, including electrons. These electrons can serve as "seeds" to facilitate plasma ignition, in turn contributing to the faster current rise. The additional charge carriers from the MW ECR sources are also responsible for the overall current increase and higher peak current compared to the pure HiPIMS discharge. As a consequence, the average power per pulse will be greater in the case of MAR-HiPIMS, at constant discharge voltage.

Ion energy- and time-resolved ToF-MS was used to characterise the ion population reaching the substrate region. By looking at the two energy-to-charge (E/Q) profiles (Fig. 6), it is possible to determine the behaviour and origin of N_2^+, N^+ and Al^+ ions. During sputtering at a relatively high peak current of 22 A in an Ar/N_2 atmosphere, the dissociation of N_2 molecules is more efficient within the HiPIMS pulsed plasma compared to the MW plasma-only measurement cycle period.

For N_2^+ dimer ions, the count rate doubled just after the pulse compared to the stable MW plasma-only conditions, whereas the N^+ atomic ion count rate was 6 times higher for HiPIMS-related ions. The dependence on the nitrogen ion count rate, for both atomic and dimer

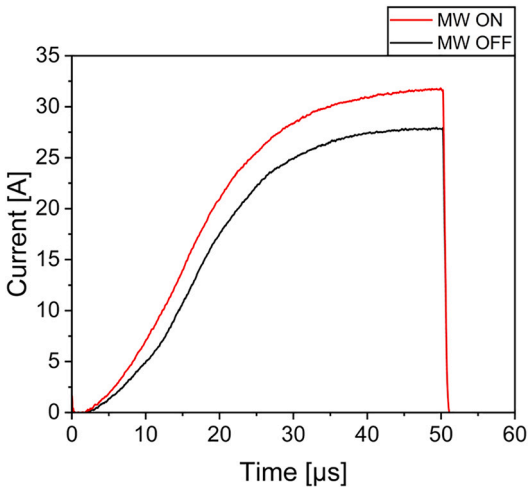

Fig. 5. Example I(V,t) curve depicting the influence of MW plasma on the shape of the discharge current during Al sputtering under Ar/N_2 conditions of 60/15 sccm, using the weaker magnet configuration in voltage-regulated mode (−750 V). Voltage regulation was chosen to highlight the difference in charges generated from the two magnets strengths, reflected in the difference in discharge current. A fixed voltage is therefore preferable, as is allows the discharge current (and therefore the average power) to vary.

ions, was proportional to the partial pressure of N_2. The count rate for nitrogen dimer ions was approximately 30 times higher than the rates for atomic nitrogen ions under MW plasma-only conditions. The opposite effect was observed by Hain *et al.* [24], where the MW plasma was more efficient than the In HiPIMS discharge in dissociating nitrogen molecules. However, in that work, much lower peak currents were attained (approx. 7 A). Nonetheless, similarly to that work, different E/Q ion groups could be distinguished, and the population of sputtered metallic species decays slowly after the end of the pulse. Especially, the high E/Q range signal from Al^+ remains close to peak value 300 µs after the end of Al pulse, motivating the choice of a 300 µs pulse duration for bias voltage.

Using the same MAR-HiPIMS technology for indium nitride deposition, the combination of the microwave plasma with low duty cycle HiPIMS plasma leads to a double peak ion energy distribution. Ions

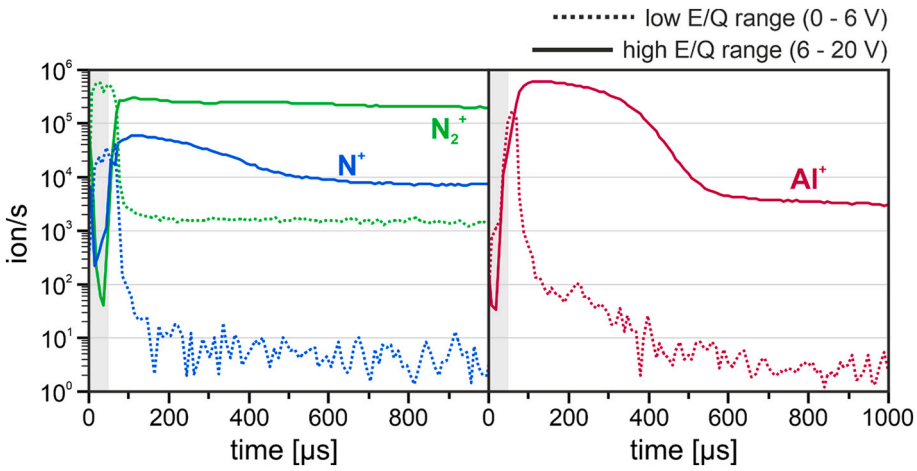

Fig. 6. Example ToF-MS profiles depicting the behaviour of N^+, N_2^+ and Al^+ for two different E/Q ranges, i.e. low E/Q range (0–6 V), associated to HiPIMS, and high E/Q range (6–20 V), related to HiPIMS + MW plasma. Discharge conditions on Al source were identical to the ones used during AlScN depositions, i.e. power regulated (200 W) at a frequency of 250 Hz, pulse width of 50 µs and a nitrogen flow of 20 sccm. The MW plasma was present for the entire measurement, whereas the duration of the HiPIMS pulse is marked in grey.

reaching the target area shortly after the end of the pulse (< 500 µs) have an energy distribution that peaks at 10 V in pure argon. This value is increased to 13 V when nitrogen was added to the carrier gas (independent of the studied N_2 flow). Later, when only the MW plasma is ignited, the peak energy increased to 12 V and 17 V for 8 and 24 sccm N_2, respectively.

During ToF-MS measurements, the presence of Al—N molecular and Al dimer ions in the gas phase was investigated. Although mass peaks were observed at 41 Th and 54 Th, they were attributed to ArH^+ and ArN^+, rather than to AlN^+ and Al_2^+, respectively. This was supported by the fact that the peak at 41 Th was also detected without the addition of N_2 to the discharge gas, whereas the peak at 54 Th disappeared.

The ToF-MS measurements using the Sc target revealed similar behaviour to the Al target. However, unlike for Al, doubly charged Sc^{2+} ions were detected in small amounts at the mass-to-charge ratio of 22.5 Th, and the peak at 59 Th was attributed to the ScN^+ molecular ion. Summarising, it can be stated that the quantity of produced ionised atomic nitrogen and those reaching the substrate is greater within the HiPIMS pulse, however, the overall production of N_2^+ is significantly higher than the generation of atomic nitrogen, at least for ionic species. In the case of Sc, the metal nitride can already be formed in the gas (plasma) phase.

3.2. AlScN films characterisation

After characterising the deposition environment, series of AlScN films were deposited, where the influence of the following parameters was investigated: *(i)* MW plasma on the chemical composition and atomic arrangement, *(ii)* substrate bias (floating vs −20 V), *(iii)* substrate heating (deposition environment temperature of approx. 150 °C vs substrate heating at 400 °C), and *(iv)* Sc contents on the AlScN films' crystalline structure and microstructure.

3.2.1. R-HiPIMS vs MAR-HiPIMS

Two AlScN thin films produced using R-HiPIMS and MAR-HiPIMS were analysed via EDX to determine the film's nitrogen and oxygen contents (see *supplementary information* for details). The film produced via R-HiPIMS exhibited an average nitrogen and oxygen content of 42 and 15 at.%, respectively. High oxygen concentrations are detrimental for the synthesis of high piezoelectric film responses [33]. The addition of MW plasma allowed to produce a film with an average N and O content of 50 and 2.7 at.%, respectively (i.e. in the EDX detection limit range for O content). Regardless of the oxygen's origin, whether incorporated during deposition or after exposure to air, the generation activated nitrogen in the microwave plasma moves the reaction balance towards the fabrication of AlScN rather than an oxide. Unlike oxygen, ground state N_2 present in ambient air and the discharge carrier gas requires plasma activation to react with Al and Sc.

The atomic structure of the deposited films was characterised by grazing-incidence XRD (GIXRD). From the X-ray diffractograms shown in Fig. 7A, it can be seen that both samples contain a single phase, i.e. the wurtzite structure, despite their significant difference in oxygen content. The atomic arrangement of the two films is similar, except at $2\theta = 36°$

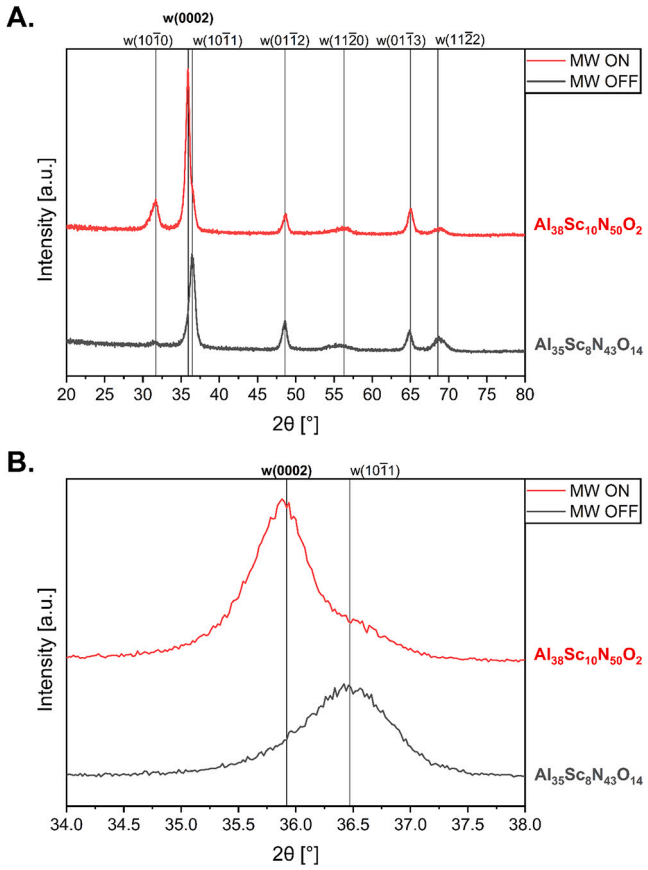

Fig. 7. A. GIXRD diffractograms of AlScN films prepared with and without MW plasma and B. Zoom-in on the $2\theta = 36°$ region. Reference peaks were assigned by simulating the AlScN diffraction spectrum using the Diffract.eva software from Bruker, USA. The diffraction peaks from hexagonal AlN (COD 1535440) were tuned until the simulated peaks overlapped measured peaks. Exact overlap was found for lattice parameters a = 3.25 Å and c = 4.99 Å; w-wurtzite. Displayed chemical compositions were characterised by EDX, see Table S1 in supplementary information for details.

where w(0002) and w(10$\bar{1}$1) peaks are found. In Fig. 7B, a clear transition from the w(10$\bar{1}$1) to w(0002) orientation is highlighted, when MW plasma is introduced into the chamber. A shoulder from the w (10$\bar{1}$1) peak is still observed on the MAR-HiPIMS sample, however, the w(0002) peak is characterised by a significantly higher intensity. The asymmetry of the peak from R-HiPIMS diffractogram also suggests the presence of w(0002) orientated grains, but in lower quantity compared to the w(10$\bar{1}$1) orientation. Additionally, the w(10$\bar{1}$0) intensity is higher for the sample prepared by MAR-HiPIMS.

This enhancement of texturing towards the w(0002) orientation emerging from the use of MW plasma can be attributed to the increased production of nitrogen ions, exhibiting higher surface mobility compared to neutral species.

3.2.2. Substrate bias vs floating potential

One of the advantages of HiPIMS is the possibility to control the behaviour of the ionised flux via substrate biasing. The studied samples were produced under the same MAR-HiPIMS conditions, with one film being deposited at floating potential, and another using a negative substrate bias of −20 V (AlN crystallinity has been reported to improve upon applying a low RF bias between −10 and -50 V [27,28]). The effects of these two conditions are visible on the surface and fracture cross-section morphologies of the fabricated AlScN films (Fig. 8).

The sample produced at floating potential possesses a “rice grain” surface structure, i.e. small and thin surface features with relatively high roughness. In contrast, the sample produced using −20 V substrate biasing shows a compact grain structure with the presence of presumably cubic rock salt structure grains (white spots), typical for AlScN. It is highly probable that these white spots have a cubic rock salt structure, which can be inferred from the morphology. Precipitates with very similar morphology have been reported in other works [3,9,11,34] and have been identified as abnormally oriented grains (AOG). The formation of AOG is attributed to the segregation of Sc to grain boundaries, with a higher AOG formation for higher Sc contents. Lu et al. [9] have reported that AOGs are characterised by a low piezoelectric amplitude and misaligned piezoelectric phase, with respect to the surrounding areas. Unfortunately, the volume fraction of these precipitates in the investigated film is below the XRD detection level. The samples' fracture cross-sections show significant differences between the two samples, where the deposition under floating potential provided strong columnar structuring while the biased film shows less pronounced columns and dense layer. Further depositions were carried out using a bias voltage of −20 V.

3.2.3. Substrate heating vs non-heating

To follow the crystallographic structure evolution of AlScN samples with varying Sc contents (selected 7, 18 and 30 at.%), two gradient films were produced. One was deposited at the temperature of the deposition environment (approx. 150 °C) and the other was fabricated while applying substrate heating (400 °C). The obtained X-ray diffractograms are presented in Fig. 9.

The diffractograms of samples containing 7 and 18 at.% Sc were characterised by a sharp peak at 36°, which corresponds to the w(0002) orientation, indicating a high degree of *c*-axis orientation both with and without substrate heating. The structure of the AlScN films drastically changes for Sc contents of 30 at.%, independent of substrate heating. The w(0002) orientation is low in intensity with significant broadening observed, whereas the intensity of the w(10$\bar{1}$1) peak intensity is increased. The apparition of c(200) and c(111) orientations are observed for the non-heated sample. A decrease in crystallinity has already been reported for samples with Sc contents exceeding 43 at.% [6,35]. However, a recent study by *Sato et al.* [36] showed that AlScN films experience a transition from wurtzite to a two-phase mixture (wurtzite + cubic phases) at approx. 30 at.% Sc, which is in good agreement with the obtained results. Next, the texture of the non-heated AlScN film containing 18 at.% Sc was investigated in greater detail by preparing a pole figure of the w(0002) reflection (Fig. 10).

Based on the presented results, the AlScN thin film deposited via MAR-HiPIMS with no additional substrate heating presented a strong out-of-plane orientation, confirmed by the pole figure measurement of the (002) diffraction peak, which also highlighted the film's fibre texture. High full width half maximum (FWHM) values from w(0002) rocking curves (not presented in this work) pointed towards significant crystallite mosaicity, most likely due to the chemical gradient present over the sample (inhomogeneous distribution of the Sc atoms might induce local variations of the crystal's microstructure). This effect may

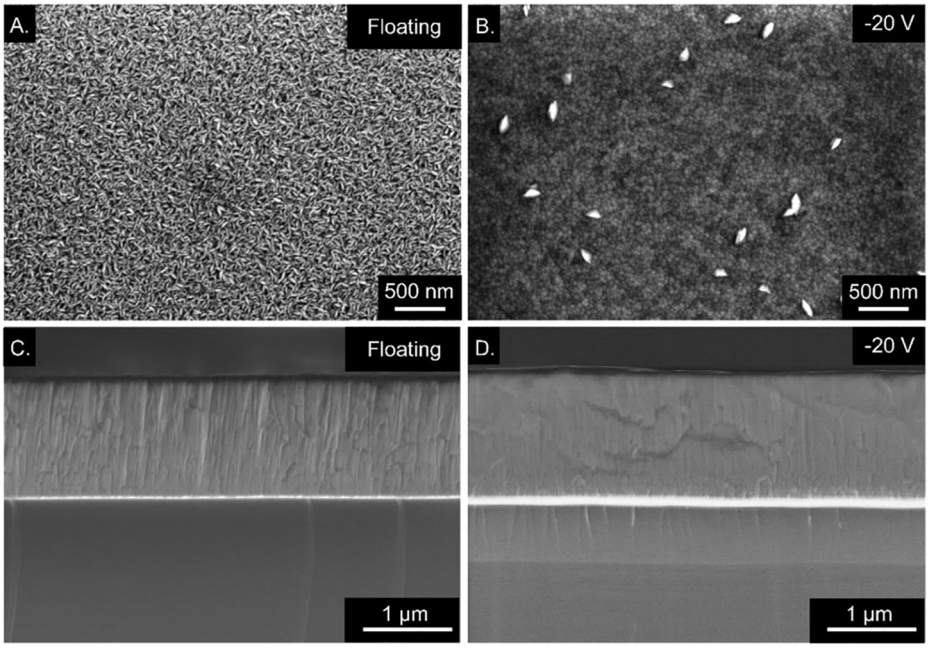

Fig. 8. SEM images of AlScN thin films produced via MAR-HiPIMS using A. and C. floating potential, B. and D. -20 V bias; The region selected for imaging presented around 20 at.% of Sc on both samples.

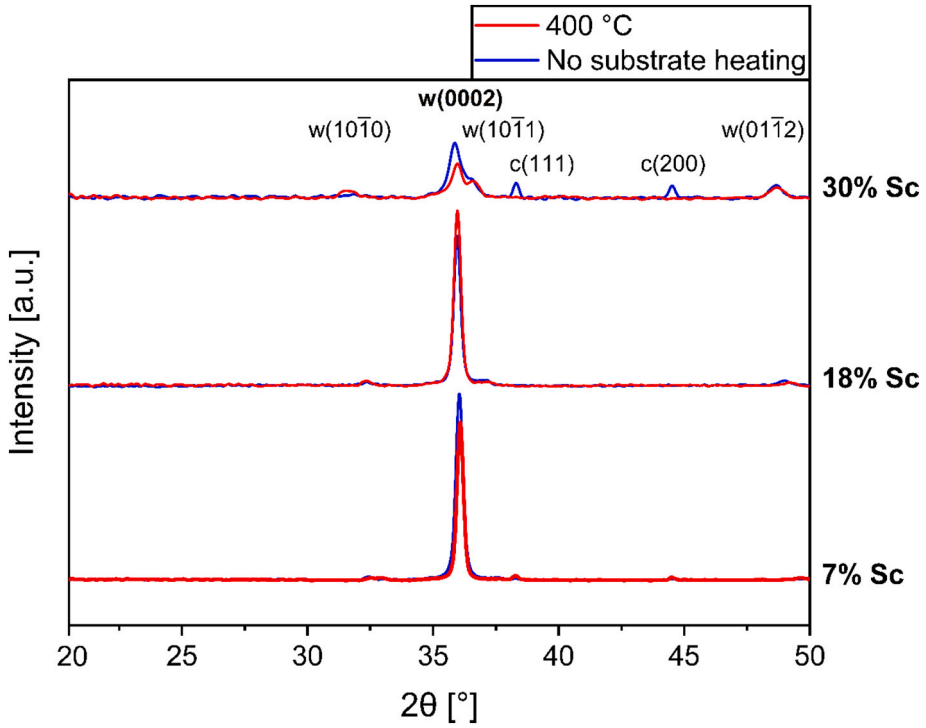

Fig. 9. θ-2θ diffractograms of AlScN films ($Al_{93}Sc_7$, $Al_{82}Sc_{18}$ and $Al_{70}Sc_{30}$ at.%) produced with and without substrate heating; reference peaks were assigned similarly to those in Fig. 8; w-wurtzite, c-cubic.

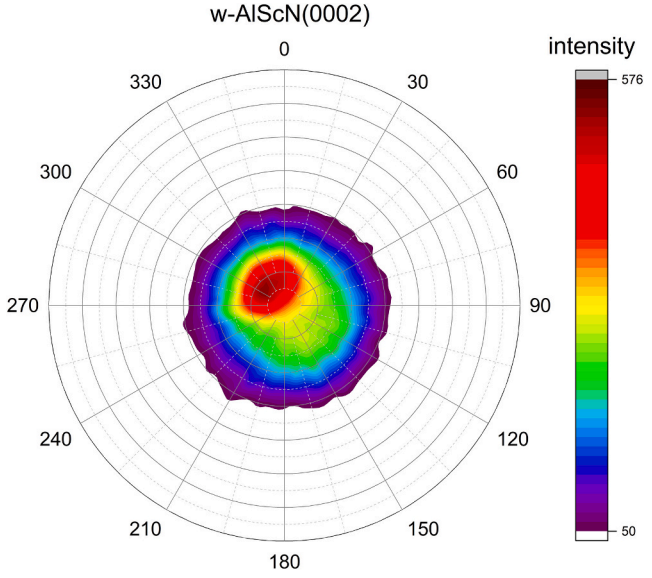

Fig. 10. Pole figure of the AlScN film's w(0002) crystalline orientation (MAR-HiPIMS, 18 at.% Sc, −20 V substrate bias, no substrate heating).

be overcome by fully rotating the sample holder during the deposition process, providing homogenous chemical composition over the entire wafer.

4. Conclusion

In this study, the MAR-HiPIMS technique, which combines microwave plasma and HiPIMS under reactive gas conditions, was used to deposit AlScN gradient films. Process diagnostic was performed to select relevant process parameters for maximising the deposition rate and ion generation from the magnetron sources. High currents enabled producing high ionised fractions, which allowed to increase the level of control over the deposition process by means of substrate biasing. Further film quality improvements were brought about with the introduction of microwave plasma, allowing for a continuous supply of activated nitrogen and enabling to reduce oxygen contaminations (<3 at.%). Films containing up to 18 at.% Sc were characterised by high crystallinity without the need of substrate heating. Significant improvement in crystallinity was not observed with substrate heating, implying that the ionic flux produced via HiPIMS and MW plasma satisfies the ad-atom surface mobility condition needed for the synthesis of oriented films. Looking at the fibre texturing of the AlScN coating in the (0002) orientation, improved by the addition of MW plasma, the films synthesised by MAR-HiPIMS are expected to provide a significant piezoelectric response. Nevertheless, to substantiate such a claim, further studies focused on the deposition and the characterisation (including piezoelectric response measurements) of homogeneous Sc-content samples is required and will be the focus of future research.

CRediT authorship contribution statement

L. Lapeyre: depositions, investigations and analysis, preparing original draft; *C. Hain*: investigations and analysis, draft revision and editing; P. Sturm: investigation and analysis, draft revision and editing; J. Metzger: investigation and analysis, draft revision and editing, *A.Borzì:* X-ray investigation and analysis, draft revision and editing; *K. Wieczerzak*: supervision, investigations and analysis, draft revision and editing; *P. Raynaud*: supervision, draft revision and editing; *J. Michler*: supervision, resources, draft revision and editing; *T. Nelis*: conceptualization, investigations, supervision, resources, draft revision and editing.

Declaration of competing interest

The authors declare no competing financial interest.

Data availability

Data will be made available on request.

Acknowledgement

This work was co-funded by the Innosuisse - Swiss Innovation Agency and the European Union as part of project E!114277 IonDrive and Innosuisse project 50631.1 INNO-ENG. K.W. was supported by the EMPAPOSTDOCS-II program that has received funding from the European Union's Horizon 2020 research and innovation program under the Marie Skłodowska-Curie grant agreement number 754364.

Appendix A. Supplementary data

Supplementary data to this article can be found online at https://doi.org/10.1016/j.surfcoat.2023.129540.

References

[1] M. Noor-A-Alam, O.Z. Olszewski, M. Nolan, Ferroelectricity and large piezoelectric response of AlN/ScN superlattice, ACS Appl. Mater. Interfaces 11 (2019) 20482–20490, https://doi.org/10.1021/acsami.8b22602.
[2] C. Fei, X. Liu, B. Zhu, D. Li, X. Yang, Y. Yang, Q. Zhou, AlN piezoelectric thin films for energy harvesting and acoustic devices, Nano Energy 51 (2018) 146–161, https://doi.org/10.1016/j.nanoen.2018.06.062.
[3] M. Akiyama, K. Kano, A. Teshigahara, Influence of growth temperature and scandium concentration on piezoelectric response of scandium aluminum nitride alloy thin films, Appl. Phys. Lett. 95 (2009) 19–22, https://doi.org/10.1063/1.3251072.
[4] M. Akiyama, K. Umeda, A. Honda, T. Nagase, Influence of scandium concentration on power generation figure of merit of scandium aluminum nitride thin films, Appl. Phys. Lett. 102 (2013), 021915, https://doi.org/10.1063/1.4788728.
[5] C.P. Huang, C.H. Wang, C.P. Liu, K.Y. Lai, High-quality AlN grown with a single substrate temperature below 1200 °c, Sci. Rep. 7 (2017) 7135, https://doi.org/10.1038/s41598-017-07616-8.
[6] S. Barth, H. Bartzsch, D. Glöß, P. Frach, T. Modes, O. Zywitzki, G. Suchaneck, G. Gerlach, Magnetron sputtering of piezoelectric AlN and AlScN thin films and their use in energy harvesting applications, Microsyst. Technol. 22 (2016) 1613–1617, https://doi.org/10.1007/s00542-015-2787-x.
[7] M. Trant, M. Fischer, K. Thorwarth, S. Gauter, J. Patscheider, H.J. Hug, Tunable ion flux density and its impact on AlN thin films deposited in a confocal DC magnetron sputtering system, Surf. Coat. Technol. 348 (2018) 159–167, https://doi.org/10.1016/j.surfcoat.2018.04.091.
[8] K.A. Aissa, A. Achour, O. Elmazria, Q. Simon, M. Elhosni, P. Boulet, S. Robert, M. A. Djouadi, AlN films deposited by dc magnetron sputtering and high power impulse magnetron sputtering for SAW applications, J. Phys. D. Appl. Phys. 48 (2015), 145307, https://doi.org/10.1088/0022-3727/48/14/145307.
[9] Y. Lu, M. Reusch, N. Kurz, A. Ding, T. Christoph, L. Kirste, V. Lebedev, A. Žukauskaitė, Surface morphology and microstructure of pulsed dc magnetron sputtered piezoelectric AlN and AlScN thin films, Phys. Status Solidi (a) 215 (2018) 1–6, https://doi.org/10.1002/pssa.201700559.
[10] M.A. Moreira, T. Törndahl, I. Katardjiev, T. Kubart, Deposition of highly textured AlN thin films by reactive high power impulse magnetron sputtering, J. Vac. Sci. Technol. A 33 (2015), 021518, https://doi.org/10.1116/1.4907874.
[11] S. Mertin, V. Pashchenko, F. Parsapour, C.S. Sandu, B. Heinz, O. Rattunde, G. Christmann, M.A. Dubois, P. Muralt, Enhanced piezoelectric properties of c-axis textured aluminium scandium nitride thin films with high scandium content: influence of intrinsic stress and sputtering parameters, in: IEEE International Ultrasonics Symposium, IUS, 2017, pp. 12–15, https://doi.org/10.1109/ULTSYM.2017.8091776.
[12] K. Umeda, H. Kawai, A. Honda, M. Akiyama, T. Kato, T. Fukura, Piezoelectric properties of ScAlN thin films for piezo-MEMS devices, in: Proceedings of the IEEE International Conference on Micro Electro Mechanical Systems (MEMS), 2013, pp. 733–736, https://doi.org/10.1109/MEMSYS.2013.6474347.
[13] M. Samuelsson, D. Lundin, J. Jensen, M.A. Raadu, J.T. Gudmundsson, U. Helmersson, On the film density using high power impulse magnetron sputtering, Surf. Coat. Technol. 205 (2010) 591–596, https://doi.org/10.1016/J.SURFCOAT.2010.07.041.
[14] A. Anders, A structure zone diagram including plasma-based deposition and ion etching, Thin Solid Films 518 (2010) 4087–4090, https://doi.org/10.1016/j.tsf.2009.10.145.
[15] S.R.C. McMitchell, A.M. Walke, K. Banerjee, S. Mertens, X. Piao, M. Mao, K. Katcko, G. Vellianitis, M. van Dal, Y.-M. Lin, G. van den Bosch, R. Delhougne, G. S. Kar, Engineering strain and texture in ferroelectric scandium-doped aluminium nitride, ACS Appl. Electron. Mater. (2023) 858–864, https://doi.org/10.1021/acsaelm.2c01421.
[16] M. Yassine, A. Nair, J. Fammels, E. Wade, Z. Fu, A. Yassine, L. Kirste, O. Ambacher, Influence of structural properties on the ferroelectric behavior of hexagonal AlScN, J. Appl. Phys. 132 (2022), 114101, https://doi.org/10.1063/5.0103578.
[17] S. Yasuoka, T. Shimizu, A. Tateyama, M. Uehara, H. Yamada, M. Akiyama, Y. Hiranaga, Y. Cho, H. Funakubo, Effects of deposition conditions on the ferroelectric properties of (Al1−xScx)N thin films, J. Appl. Phys. 128 (2020), 114103, https://doi.org/10.1063/5.0015281.
[18] C. Takahashi, M. Kiuchi, T. Ono, S. Matsuo, An electron cyclotron resonance plasma deposition technique employing magnetron mode sputtering, J. Vac. Sci. Technol. A 6 (1988) 2348–2352, https://doi.org/10.1116/1.575588.
[19] J. Musil, S. Kadlec, W.-D. Münz, Unbalanced magnetrons and new sputtering systems with enhanced plasma ionization, J. Vac. Sci. Technol. A 9 (1991) 1171–1177, https://doi.org/10.1116/1.577597.
[20] J.T. Gudmundsson, Ionized physical vapor deposition (IPVD): magnetron sputtering discharges, J. Phys. Conf. Ser. 100 (2008), 082002, https://doi.org/10.1088/1742-6596/100/8/082002.
[21] J.T. Gudmundsson, Physics and technology of magnetron sputtering discharges, Plasma Sources Sci. Technol. 29 (2020), 113001, https://doi.org/10.1088/1361-6595/abb7bd.
[22] V. Stranak, A.P. Herrendorf, S. Drache, M. Cada, Z. Hubicka, R. Bogdanowicz, M. Tichy, R. Hippler, Plasma diagnostics of low pressure high power impulse magnetron sputtering assisted by electron cyclotron wave resonance plasma, J. Appl. Phys. 112 (2012), 093305, https://doi.org/10.1063/1.4764102.
[23] V. Stranak, Z. Hubicka, M. Cada, S. Drache, M. Tichy, R. Hippler, Investigation of ionized metal flux in enhanced high power impulse magnetron sputtering discharges, J. Appl. Phys. 115 (2014), 153301, https://doi.org/10.1063/1.4871635.
[24] C. Hain, P. Schweizer, P. Sturm, A. Borzì, J.E. Thomet, J. Michler, A. Hessler-Wyser, T. Nelis, Microwave plasma-assisted reactive HiPIMS of InN films: plasma environment and material characterisation, Surf. Coat. Technol. 454 (2023), 129188, https://doi.org/10.1016/j.surfcoat.2022.129188.
[25] J.T. Gudmundsson, On reactive high power impulse magnetron sputtering, Plasma Phys. Controlled Fusion 58 (2015), 014002, https://doi.org/10.1088/0741-3335/58/1/014002.
[26] L. Latrasse, M. Radoiu, T. Nelis, O. Antonin, Self-matching plasma sources using 2.45 GHz solid-state generators: microwave design and operating performance, J. Microw. Power Electromagn. Energy 51 (2017) 237–258, https://doi.org/10.1080/08327823.2017.1388338.
[27] F. Zoubian, N. Renaut, L. Latrasse, Distributed elementary ECR microwave plasma sources supplied by solid state generators for production of large area plasmas without scale limitation: plasma density measurements and comparison with simulation, Plasma Res. Express 3 (2021), 025010, https://doi.org/10.1088/2516-1067/ac0499.
[28] S. Sharma, D. Gahan, P. Scullin, J. Doyle, J. Lennon, R.K. Vijayaraghavan, S. Daniels, M.B. Hopkins, Measurement of deposition rate and ion energy distribution in a pulsed dc magnetron sputtering system using a retarding field analyzer with embedded quartz crystal microbalance, Rev. Sci. Instrum. 87 (2016), 043511, https://doi.org/10.1063/1.4946788.
[29] N. Brenning, A. Butler, H. Hajihoseini, M. Rudolph, M.A. Raadu, J. T. Gudmundsson, T. Minea, D. Lundin, Optimization of HiPIMS discharges: the selection of pulse power, pulse length, gas pressure, and magnetic field strength, J. Vac. Sci. Technol. A 38 (2020), 033008, https://doi.org/10.1116/6.0000079.
[30] M. Rudolph, N. Brenning, H. Hajihoseini, M.A. Raadu, T.M. Minea, A. Anders, J. T. Gudmundsson, D. Lundin, Influence of the magnetic field on the discharge physics of a high power impulse magnetron sputtering discharge, J. Phys. D. Appl. Phys. 55 (2022), 015202, https://doi.org/10.1088/1361-6463/ac2968.
[31] M.A. Lewis, D.A. Glocker, J. Jorne, Measurements of secondary electron emission in reactive sputtering of aluminum and titanium nitride, J. Vac. Sci. Technol. A 7 (1989) 1019–1024, https://doi.org/10.1116/1.576222.
[32] M. Fekete, K. Bernátová, P. Klein, J. Hnilica, P. Vašina, Evolution of discharge parameters and sputtered species ionization in reactive HiPIMS with oxygen, nitrogen and acetylene, Plasma Sources Sci. Technol. 28 (2019), 025011, https://doi.org/10.1088/1361-6595/AB0363.
[33] M. Akiyama, T. Kamohara, K. Kano, A. Teshigahara, N. Kawahara, Influence of oxygen concentration in sputtering gas on piezoelectric response of aluminum nitride thin films, Appl. Phys. Lett. 93 (2008) 2006–2009, https://doi.org/10.1063/1.2957654.
[34] C.S. Sandu, F. Parsapour, S. Mertin, V. Pashchenko, R. Matloub, T. LaGrange, B. Heinz, P. Muralt, Abnormal grain growth in AlScN thin films induced by complexion formation at crystallite interfaces, Phys. Status Solidi (a) 216 (2019) 1–11, https://doi.org/10.1002/pssa.201800569.
[35] O. Zywitzki, T. Modes, S. Barth, H. Bartzsch, P. Frach, Effect of scandium content on structure and piezoelectric properties of AlScN films deposited by reactive pulse magnetron sputtering, Surf. Coat. Technol. 309 (2017) 417–422, https://doi.org/10.1016/j.surfcoat.2016.11.083.
[36] S. Satoh, K. Ohtaka, T. Shimatsu, S. Tanaka, Crystal structure deformation and phase transition of AlScN thin films in whole sc concentration range, J. Appl. Phys. 132 (2022), 025103, https://doi.org/10.1063/5.0087505.